Sustainable Cities and Society 101 (2024) 105116

Contents lists available at ScienceDirect

Sustainable Cities and Society

journal homepage: www.elsevier.com/locate/scs

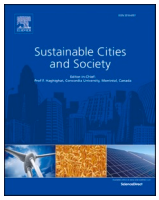

The effects of 2-D and 3-D urban landscape metrics on mean radiant temperature in hot-arid Phoenix and Tempe, Arizona, USA

Ahmet Cilek [a,b,*], Muge Unal [a,c], Ariane Middel [a]

[a] School of Arts, Media and Engineering (AME), Arizona State University, 85281 Tempe, AZ, United States
[b] Cukurova University, Landscape Architecture Department, Remote Sensing and GIS Lab, 01330, Adana, Turkey
[c] Firat University, Faculty of Architecture, Landscape Architecture Department, 23119, Elazig, Turkey

ARTICLE INFO

Keywords:
Thermal exposure
Landscape metrics
MRT
Urban thermal environment
3-D urban landscape metrics

ABSTRACT

The composition and configuration of the built environment affect intra-urban heat variability and human thermal exposure. We investigated how 2-D and 3-D building and vegetation characteristics, represented by various landscape metrics, affect the mean radiant temperature (MRT) distribution in Phoenix and Tempe, Arizona, USA, to determine which urban form characteristics are most important for minimizing thermal exposure. For a hot-dry summer day with low wind speed and a maximum air temperature of 43.3 °C, the relationship between 1-m resolution MRT data and seventeen 2-D and 3-D landscape metrics were analyzed at the Census block (micro) and urban (macro) scale. The landscape metrics were calculated with FragStat from a Digital Surface Model, a 3-D point cloud obtained from high-resolution (0.5-m) USGS LiDAR data, and a 1-m resolution land use/land cover map classified from the 2015 National Agriculture Imagery Program (NAIP) data. Hourly MRT for June 27, 2012, was simulated using the SOlar LongWave Environmental Irradiance Geometry (SOLWEIG) model. After testing for autocorrelation in hourly MRT using Moran's I, the relationship between landscape metrics and MRT outcomes was analyzed using correlation coefficients and multiple linear regression. The best predictive power was achieved using 2-D and 3-D metrics together, with an explanation MRT of 86 % (8:00 h) to 96 % (12:00 h). The five most important factors were 3-D vegetation height, 2-D percent tree surface cover, 3-D building height, 2-D building edge density, and the 3-D vegetation height coefficient of variation. Results show that MRT is driven by the composition and configuration of 2-D and 3-D urban features. The horizontal arrangement impacts MRT through varying land cover, and the vertical extent influences shade patterns, with more complex urban forms providing more shade and lowering MRT. Findings advance our understanding of how urban design can reduce thermal exposure on hot days using passive cooling strategies that rely on changes in the configuration and composition of landscapes.

1. Introduction

Urbanization, one of the most visible impacts of human activity on Earth, significantly affects the local climate in cities (Kalnay et al., 2004; Oke et al., 2017). Buildings, roads, and other impermeable surfaces alter natural landscapes during urbanization, resulting in fragmented and complex landscapes (Kalnay & Cai, 2003; Yu et al., 2016). Urbanization negatively impacts various urban systems, including air quality (Duh et al., 2008; Han et al., 2014; Santamouris, 2013) and stormwater runoff (Bhaduri et al., 2001; Papagiannaki et al., 2015). Converting natural to built environments also significantly affects the urban thermal environment (UTE) (Alberti & Marzluff, 2004; Cai et al., 2017; Charalampopoulos et al., 2013; Johansson & Emmanuel, 2006; Kong et al., 2022; Li et al., 2020; Perkins et al., 2012; Solcerova et al., 2017; Xian & Crane, 2006). High temperatures reduce thermal comfort, especially in the absence of shade (Middel et al., 2016; Kelly Turner et al., 2023), and increase the risk of heat stress and mortality (Chow et al., 2011; Harlan et al., 2006; Hondula et al., 2014). These circumstances have led to increased awareness of the effects of land cover composition and configuration on human health and activity (Li et al., 2016; Middel et al., 2014; Myint et al., 2013; Zhang et al., 2018).

Previous research has identified changes in land use and land cover (LULC) as critical drivers of UTE degradation (Deilami et al., 2018). Investigating how the local urban landscape structure affects UTE

* Corresponding author at: School of Arts, Media and Engineering (AME), Arizona State University, 85281 Tempe, AZ, United States.
E-mail address: acilek@cu.edu.tr (A. Cilek).

https://doi.org/10.1016/j.scs.2023.105116
Received 24 July 2023; Received in revised form 10 December 2023; Accepted 10 December 2023
Available online 16 December 2023

variability is crucial to developing targeted heat mitigation strategies and promoting sustainable urban and regional development (Zhou et al., 2022a). While the field of urban climate has investigated the urban heat island (UHI) and its relationship to urban form for many decades (Nichol, 1996; Unger, 2009; Middel et al., 2014; Wang et al., 2023), few studies have focused on the impact of urban morphology on human-centric thermal exposure, quantified as mean radiant temperature (MRT).

Landscape metrics quantify the composition and configuration of landscape features, such as patch types and their spatial arrangement (McGarigal et al., 2002; Yu et al., 2020). Researchers have previously explored the relationship between land system architecture and climatic characteristics at different scales by evaluating two-dimensional (2-D) LULC and landscape metrics (Berger et al., 2017; Deilami et al., 2018; Estoque et al., 2017; Sun et al., 2020a, Guo et al., 2020; Masoudi et al., 2021; Sun et al., 2018; Tian et al., 2019). Studies focusing on the effects of 2-D landscape metrics employed patch density (PD), edge density (ED), landscape shape index (LSI), largest patch index (LPI), mean patch size (AREA_MN), mean patch shape index (SHAPE_MN) and contamination index (CONTAG) to investigate impacts on Land Surface Temperature (LST) (Amiri et al., 2009; Huang & Wang, 2019; Li et al., 2011, 2016; Siqi & Yuhong, 2020; Zhou et al., 2017). However, 2-D urban landscape metrics insufficiently capture the vertical heterogeneity of cities, which affects shading patterns and therefore heat storage in the built environment (Deilami et al., 2018; Zhou et al., 2017). Researchers have started to analyze landscape metrics in 3-D to understand the dynamic thermal processes within and between landscape fragments (Yan et al., 2019; Zhou et al., 2022b; Stewart & Oke, 2012). Using advanced 3-D data technology such as LiDAR allows to explore this relationship (Getzner et al., 2016; Li et al., 2016; Luan et al., 2020; Petras et al., 2017; Wu et al., 2012; Zimble et al., 2003). For example, the 3-D characteristics of vegetation, such as tree height and crown shape, significantly impact the UTE at the microscale (Chun & Guldmann, 2018; Zellweger et al., 2019; Zhang et al., 2019) through increased shading and evapotranspiration (Alexander, 2021; Chen et al., 2019; Yu et al., 2018). Research has shown that increasing vegetation alone cannot fully meet the large-scale cooling demand of a city (Bowler et al., 2010; Kong et al., 2022; Norton et al., 2015; Wong & Yu, 2005), and passive cooling strategies that involve the configuration of landscapes, not just the composition, should be explored.

Past studies have primarily relied on LST to represent the thermal variability in cities, but LST has limited applications for human thermal experiences. The radiative fluxes that the human body is exposed to outdoors significantly drive thermal exposure. MRT is one of the most important meteorological parameters that affect thermal exposure (Middel et al., 2021; Schneider et al., 2023; Thorsson et al., 2007). MRT considers the radiative fluxes of the Sun, ground surfaces, building facades, and vegetation, allowing it to more thoroughly represent how a person experiences thermal conditions, particularly in hot, dry areas (Middel & Krayenhoff, 2019). Radiative flux models such as SOLWEIG (Lindberg et al., 2008) model MRT for urban areas at high spatial resolution.

In summary, previous studies have used 2-D and 3-D landscape metrics to investigate the impact of urban morphology on UTEs but mainly focused on coarse LST, not human-relevant heat metrics such as MRT. It is challenging to develop generalized urban design guidelines to improve the thermal environment based on LST alone (Huang & Wang, 2019; Yin et al., 2019; Yu et al., 2020, 2021). High-resolution spatial MRT or similar human-centric data at different times of day are needed to address this gap.

This study evaluates the effects of 2-D and 3-D urban landscape patterns (configuration and composition) on thermal exposure (MRT) at local and hyperlocal scales. We aim to find the urban form characteristics that most strongly impact MRT to advance understanding of how urban design can reduce thermal exposure on hot days using passive cooling strategies that rely on changes in the configuration and composition of landscapes.

2. Materials and methodology

2.1. Study area

This study was conducted in Phoenix (33°27′1.70″N, −112°4′26.5″W) and Tempe (33°25′28.6″N, −111°56′18.6″W) in Maricopa County, Arizona, USA (Fig. 1). Phoenix, the capital of the State of Arizona, is the fifth most populous city in the USA, with a population of 4652,000 in 2022. The study area covers 176.6 km^2, with 70.1 km^2 comprising central Phoenix and 106.5 km^2 comprising the City of Tempe. The metropolitan area is known for its urban sprawl, with a population density of approximately 1200 people per square kilometer. The urban centers consist primarily of open and partially compact midrise to high-rise Local Climate Zone (LCZ) classes, while the outskirts have open low-rise buildings with a lower-density development pattern. The southern part of the City of Tempe has one- to two-story single-family homes and lower-density residential developments (LCZ 6, open low-rise), strip malls (LCZ8, large low-rise), and office parks (LCZ5, open-midrise) (Wang et al., 2018). The city center in the north is transitioning from an open low/mid-rise to an open mid/high-rise area, with three- to four-story office and commercial buildings and several new apartment complexes and hotels under construction. Percent tree cover is low; vegetation mainly consists of small trees, shrubs, and grass (Wang et al., 2018). The presence of vegetation and open green spaces beyond residential plots, such as parks and golf courses, varies by neighborhood across the city (Harlan et al., 2006). Due to rapid urban expansion, the majority of urban forms in the metropolitan area consist of open-spaced, low to mid-rise buildings (i.e., low building height and density) and broad streets with a high sky view factor (SVF) (Middel et al., 2018; Wang et al., 2018).

The Phoenix metropolitan area, located northeast of the Sonoran Desert, has a semi-arid climate (Köppen-Geiger BWh (Kottek et al., 2006) with annual precipitation of 237 mm and low humidity of 31 %. Most of the rainfall occurs in July and August (62 mm) and during the winter months (December-March, 112 mm), while June is exceptionally dry with less than 1 mm of precipitation. Phoenix is one of the hottest cities in the USA, with an average high temperature of over 39.4 °C during the summer months and 110 days above this temperature (National Weather Service, 2018). Maximum temperatures peak close to 50 °C in the summer, while nighttime lows typically range between 27 °C and 29 °C (Western Regional Climate Center, 2020). In winter, mean daily high temperatures are above 13 °C, and minimum temperatures are rarely below 4 °C.

The synoptic macroclimate, geography, and urban patterns have created a pronounced Urban Heat Island (UHI) over the past 60 years (Chow et al., 2012). Impermeable surface areas in the metropolitan region have increased significantly since the mid-twentieth century. Rapid and extensive urbanization has raised nighttime temperatures by about 0.5 °C per decade since 1910. By the end of the 20th century, the average daily air temperature had increased by 3.1 °C and the minimum night temperature by 5.0 °C (Brazel et al., 2000; Kane et al., 2014; Sha & Tian, 2010; Shrestha et al., 2012).

2.2. Data

We utilized 5143 census blocks (2385 in Phoenix and 2758 in Tempe) from the 2010 Census in the downtown areas of Phoenix and Tempe, where developments are concentrated. These census block data were utilized as a unit of analysis to generate 2-D and 3-D landscape metrics at the neighborhood (or local) scale. Three remote sensing datasets were used to generate the landscape metrics and estimate MRT: a Digital Surface Model (DSM), Vegetation/Building Heights (H_v and H_b), and a Land Use Land Cover (LULC) map. DSM, H_v, and H_b were derived from 2014 LIDAR data with a spatial resolution of 0.5-m. The

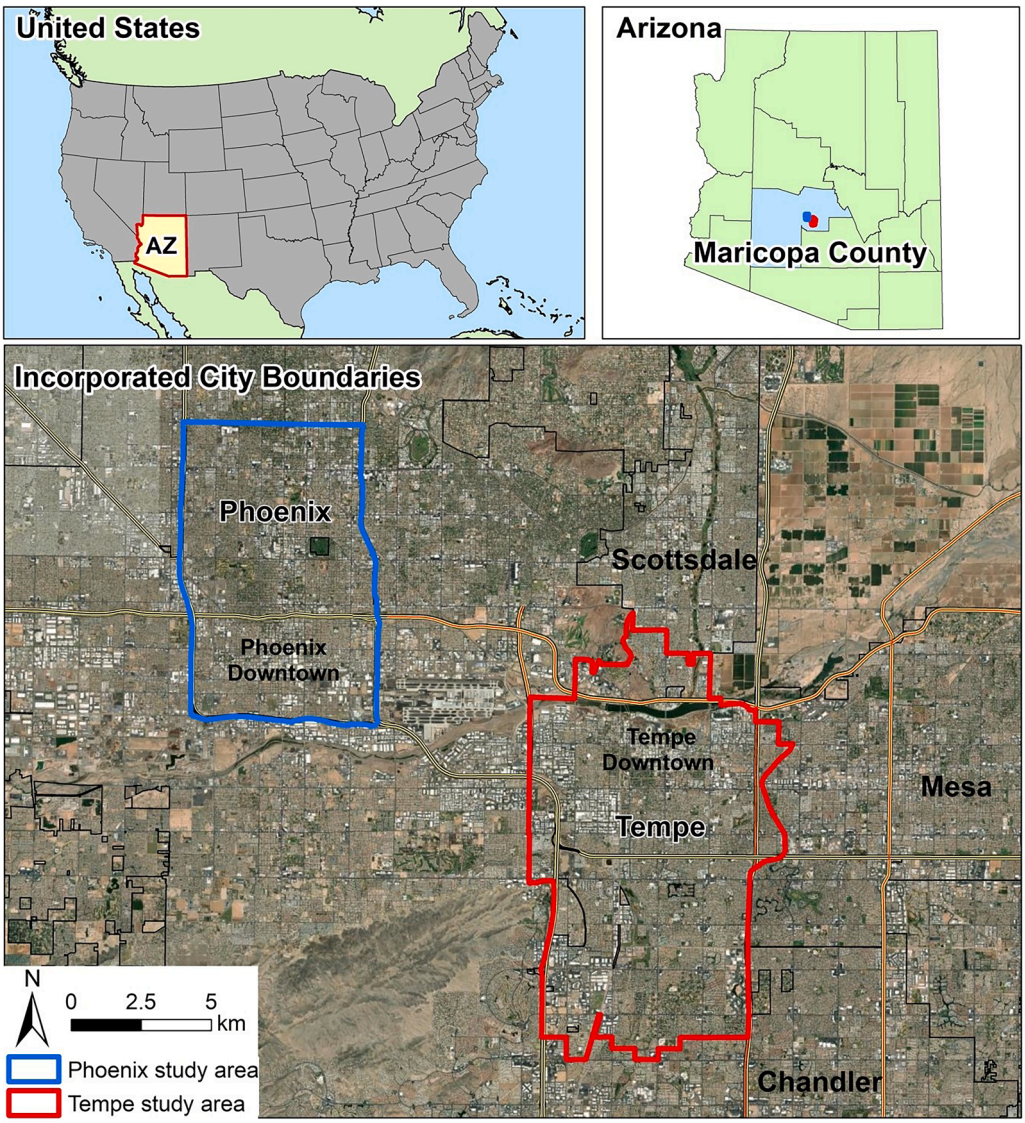

Fig. 1. Study areas in the City of Phoenix and the City of Tempe, Arizona, USA.

LULC map was created by classifying 1-m resolution National Agriculture Imagery Program (NAIP) data from 2015 into eight land cover classes: (1) building, (2) asphalt, (3) bare soil and concrete, (4) trees and shrubs, (5) grass, (6) water, (7) agricultural fields, and (8) fallow land (Zhang & Turner, 2020). The LULC classification was used to calculate the 2-D landscape metrics for this study, excluding agricultural fields and fallow land.

We retrieved hourly MRT data for the Phoenix metropolitan region from Buo et al. (2023), who simulated MRT at 1-m spatial resolution for a clear and hot summer day on June 27, 2012, using the SOlar and LongWave Environmental Radiation Geometry (SOLWEIG) model. SOLWEIG predicts short-wave and long-wave radiation fluxes based on urban geometry, such as SVF (Lindberg et al., 2008; Ratti et al., 2006), vegetation, geographic information (latitude, longitude, and altitude), and meteorological forcing data (direct and diffuse radiation, global radiation, air temperature, and relative humidity). SOLWEIG creates a virtual 3D model that includes information about the height, width, and orientation of buildings and other objects. The shadow casting algorithm in the SOLWEIG model determines whether a specific pixel within the model domain experiences shading, distinguishing between shade from vegetation and buildings. This virtual model allows calculating short-wave and long-wave radiation fluxes from six directions (north, south, east, west, zenith, and nadir) for each raster point in the model domain. The MRT is then calculated as the weighted average of the radiant temperatures of all surfaces visible from the reference point. The weights are determined by the proportion of sky visible from each surface. This calculation considers direct solar radiation, diffuse solar radiation, and long-wave radiation from the sky and surrounding surfaces (Lindberg et al., 2008).

Buo et al. (2023) extensively validated the SOLWEIG model in Phoenix and Tempe using 763 observations with a mobile human-biometeorological 6-way setup (Middel et al., 2019). The observations were conducted from 07:00 h to 21:00 h Local Standard Time (LST) across nine warm summer days in the years 2016, 2018, and 2019 (Middel et al., 2021). Biometeorological data were obtained in various areas, including beneath trees, within building canyons, and at open sites. The model validation revealed a strong relationship between the modeled and observed MRT, with an R^2 value of 0.91 and a high index of agreement (0.95). The MRT estimates had an overall RMSE of 5.6 °C, with errors of 6.2 °C in open areas, 5.4 °C under trees, and 4.4 °C in building canyons. These MRT estimates are close to the accuracy requirements defined in the ISO7726 standard. The model tends to overestimate MRT in shaded locations, a limitation previously acknowledged by Szucs et al. (2014) and Gal and Kantor (2020). Gal and Kantor (2020)

attribute the overestimations in shaded areas to the use of domain-wide surface temperature for determining longwave radiation and the theoretical approach employed by the model in estimating fluxes from sun-exposed and shaded walls. Additionally, an inherent dataset imbalance, characterized by a higher number of observations in shaded/tree environments, contributes to the overall overestimation. We retrieved Buo et al. (2023)'s hourly MRT raster data for four different times of the day (08:00 h, 12:00 h, 16:00 h, and 20:00 h) and aggregated the data to Census blocks.

2.3. Analysis

The analysis comprises three steps (Fig. 2). First, 2-D and 3-D landscape metrics were calculated using the DSM and LULC data for each Census block to quantify the composition and configuration of land cover patches. Second, MRT was modeled with SOLWEIG (Buo et al., 2023). Third, a stepwise regression analysis was conducted to analyze the relationship between the landscape metrics and MRT.

2.3.1. Selecting metrics & metric calculation

Landscape composition and configuration describe the spatial patterns and relationships between different elements in a landscape (Liu et al., 2017a; Sun et al., 2020b; Zeng et al., 2022). We propose a comprehensive set of 2-D and 3-D landscape metrics to evaluate these patterns in the urban environment because landscape structure and urban form influence local climate dynamics and microscale MRT. Many 2-D landscape metrics are available in the literature (Baker & Cai, 1992; Frazier & Kedron, 2017). A set of metrics is generated at the patch, class, and landscape level in FRAGSTATS, including various area metrics, patch density, size and variability metrics, edge metrics, shape metrics, core area metrics, diversity metrics, and contamination and scattering metrics. We calculated all 2-D metrics in FRAGSTATS at the class and landscape level and excluded the highly correlated ones. A cluster analysis was initially conducted to group the factors to ensure the non-redundancy and representability of these factors (Chen et al., 2016). Subsequently, backward selection algorithms based on the maximum relevance principle were employed to rank these metrics according to their relative importance and select representative metrics of significance within each group (Li et al., 2021). Metrics relating to the composition of land cover include area types such as class area, percent surface types (e.g., percent impervious), and mean fractal dimension index (measures the complexity of the landscape patch). 2-D metrics related to configuration include edge density (ED), aggregation-type metrics such as the number of patches (NP), splitting index (SPLIT), contagion (CONTAG), and shape indices (e.g., mean contiguity). For a complete list, please see Table A1.

The 3-D landscape metrics were grouped into two categories: (1) 3-D landscape composition metrics and (2) elevation-based metrics (Table A2). The first category was extended from traditional 2-D metrics but calculated in 3-D space. In the second category, we adopted the methods of Wu et al. (2017) to combine 2-D landscape metrics with 3-D terrain surfaces by introducing 3-D area and length calculations. Building and vegetation height were obtained from high-precision LiDAR data. These metrics are commonly used in related research (Ke et al., 2022). We calculated four 3-D landscape composition metrics and ten 3-D elevation metrics. To combine 2-D and 3-D landscape pattern metrics, the evenness index and patch index were calculated in 3-D based on building and vegetation height.

The type of landscape metrics is named C or L for class or landscape, followed by 2-D or 3-D. For example, 2D-C denotes class-level metrics in 2-D. The descriptions of each landscape metric are shown in Table A2 (Yu et al., 2021). Metrics describe building characteristics such as height, volume, shape, and density and have been shown to affect the UTE (Alavipanah et al., 2018; Berger et al., 2017).

2.3.2. Statistical analyses

Several statistical analyses were conducted to explain the relationship between hourly MRT and landscape metrics aggregated at the Census block level. First, a bivariate correlation analysis was applied to all landscape metrics to determine which metrics to exclude. Second, to

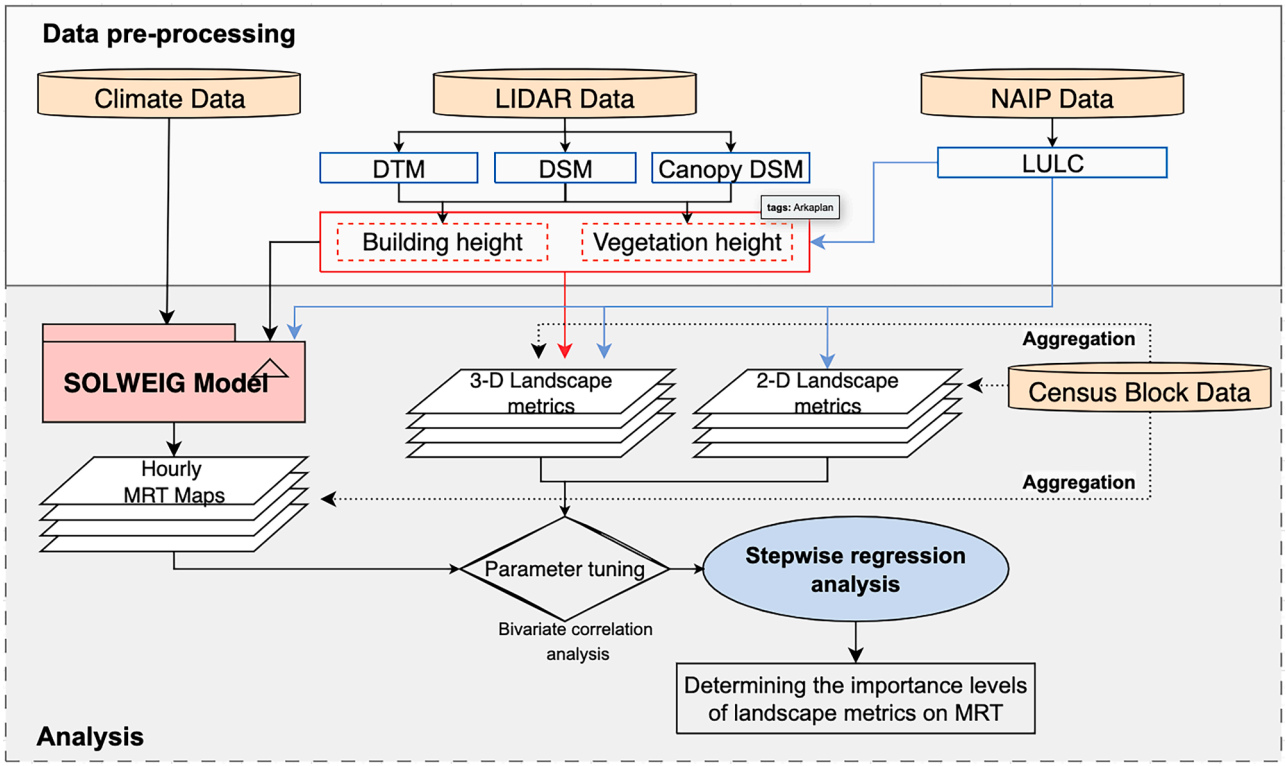

Fig. 2. Flowchart of the implementation and analysis.

understand the spatial distribution of MRT, we used Global Moran's I to quantify the spatial autocorrelation of MRT at different times of day. Global Moran's I is a statistical measure to quantify geographical autocorrelation, which is the degree to which the values of a variable in a global dataset are similar or dissimilar (Bivand & Piras, 2015; Fu et al., 2014). The index ranges from −1 to 1, with 1 indicating perfect spatial autocorrelation, −1 indicating perfect negative spatial autocorrelation, and 0 indicating no spatial autocorrelation. Global Moran's I was calculated in GeoDa using first-order queen contiguity weights as the spatial weight matrix. Third, we utilized a partial correlation analysis (Wang et al., 2006) to investigate the correlation between MRT and the landscape metrics. Partial correlation analysis evaluates the strength of the linear correlation between two variables while considering the influence of other variables (Xiao et al., 2022). The closer the correlation coefficient is to 1, the stronger the correlation between variables; the closer it is to 0, the weaker the correlation. Factors with low correlation ($R^2 < 0.2$) between the indices and MRT were excluded.

Finally, stepwise multiple regression analysis was adopted to find the independent and interactive effects of the selected metrics on MRT. Each variable was normalized to eliminate the size effect in the regression analysis. Then, stepwise multiple regression analysis was performed to determine the relative importance of the variable. The highest correlation coefficient (R^2) was used for the optimal result (Zhan et al., 2013). 3-D and 2-D landscape metrics served as independent variables, and MRT values at four selected hours were used as dependent variables in the regression.

Multicollinearity is a common problem when two or more predictive variables are highly correlated in regression analysis. When multicollinearity is present, it can lead to biased and unreliable regression coefficients, which may ultimately affect the accuracy of the model's predictions (Stevens, 2009). Therefore, the variance inflation factor (VIF) (Asgarian et al., 2015; Guo et al., 2019) was applied to evaluate the

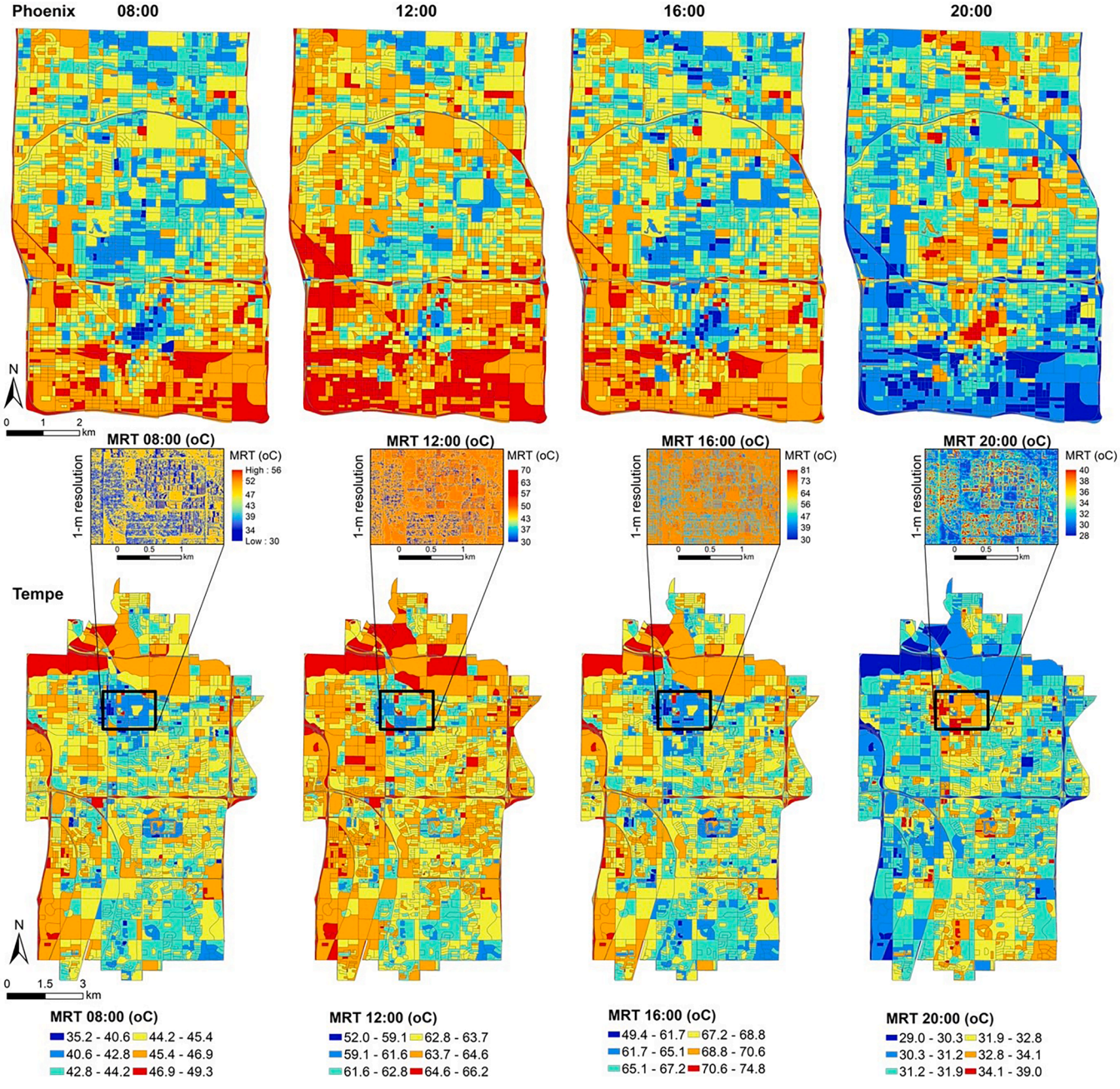

Fig. 3. Hourly MRT maps; results are aggregated at the Census block scale; the small maps in the center show 1-meter results for a sub-area.

collinearity in independent variables in the models with variables having a VIF value equal to or exceeding 7.5 (Guo et al., 2020; Shen et al., 2022) being excluded from the model.

3. Results

3.1. Spatial MRT distribution in the study area

The average hourly MRT at the Census block level over the study area for June 27, 2012, varied widely across space during the day and peaked at 61 °C at 15:00 h and 16:00 h in some blocks. MRT then decreased and became more homogeneous spatially after sunset in the absence of shade. MRT values in vegetated Census blocks were consistently +3 to +5 °C lower than in bare neighborhoods. During midday, residential areas experienced an increase in MRT because shading was minimal. In contrast, north-south oriented streets were mostly shaded by tall buildings in the afternoon, reducing direct solar radiation and heat storage (e.g., downtown Phoenix and Tempe with low SVF). Average MRT was lower in densely built-up areas with reduced SVF, but longwave radiation was trapped near the ground after sunset (Fig. 3).

Moran's I values for MRT ranged between −1 (dispersed) and 1 (clustered). The spatial autocorrelation determines whether high or low average MRT values in a Census block increase the probability of similarly high or low values in the surrounding blocks. The hourly Moran's I values for MRT for 08.00 h, 12.00 h, 16.00 h, and 20.00 h were 0.50, 0.45, 0.45, and 0.51, respectively (Fig. 4). According to these results, almost half of the area exhibits spatial autocorrelation. The Census blocks were categorized into four groups: high-high (H—H), low-low (L-L), high-low (H-L), and low-high (L-H). The H—H type represents clusters of high MRT values, the l-L type indicates clusters of low MRT values, and the H-L (L-H) type represents a cluster of low (high) MRT values around a high (low) MRT block. During the day, south Phoenix exhibited H—H local Moran I clusters, while the l-L type was concentrated in the central and northern parts of the area. Cluster types reversed after sunset (20:00 h). In Tempe, the H—H type was spread along the I-10 highway from north to south and the Tempe Lake area to the north. The l-L type was found in Tempe's downtown and southern neighborhoods. In addition, few l-H and H-L types were spread across the two cities (Fig. 4).

3.2. 2-D/3-D landscape metrics and MRT response

At the landscape level, 27 2D metrics were generated. Since many of these metrics were highly correlated, a bivariate correlation analysis

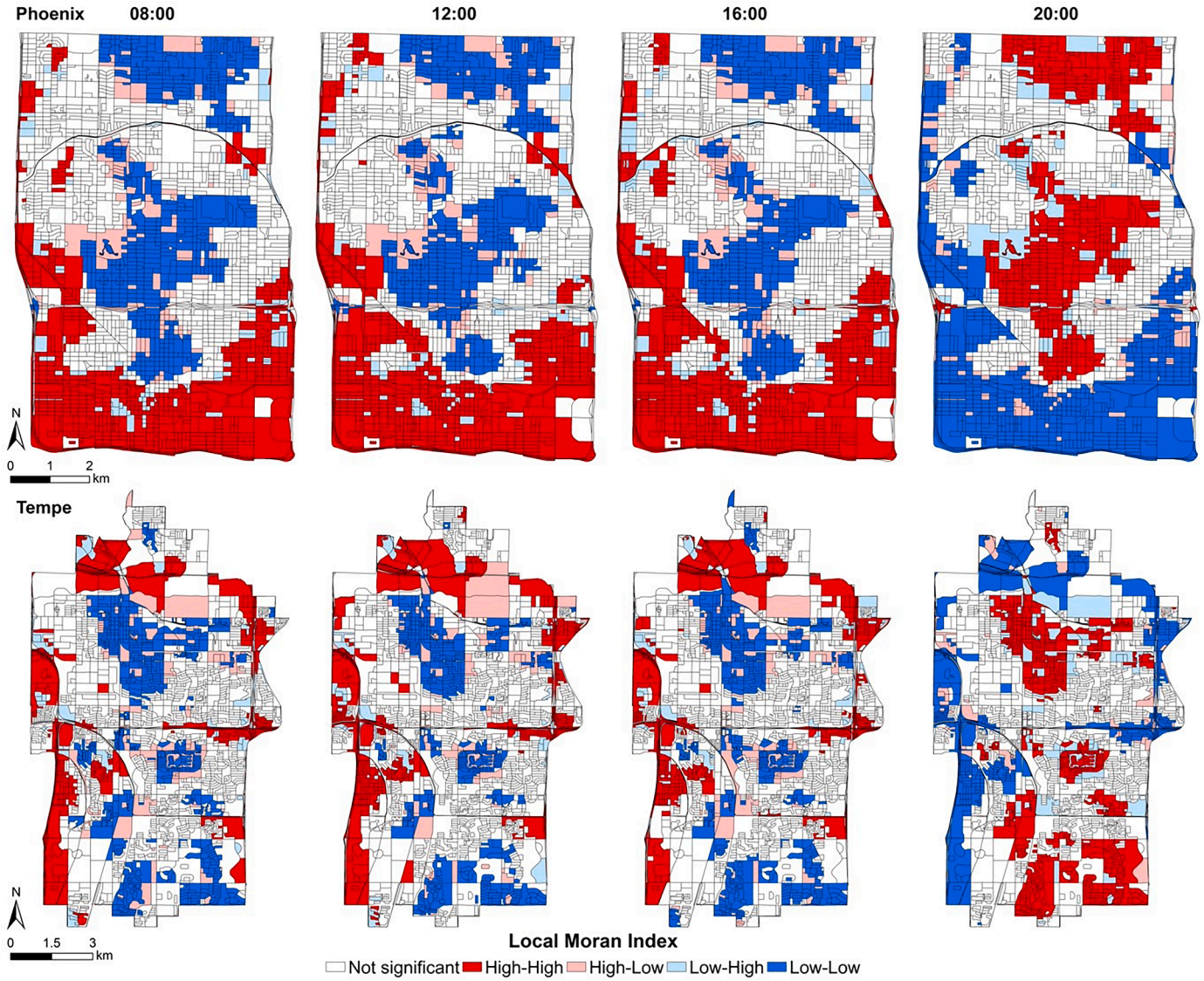

Fig. 4. Local moran index for hourly MRT results at the census block level.

was applied, and nine 2-D landscape metrics were selected as dependent variables (Table A1): Mean fractal dimension index (FRAC_MN), Edge density (ED), Number of patches (NP), Patch density (PD), Splitting index (SPLIT), Contagion (CONTAG), Effective mesh size (MESH), Mean contiguity index (CONTIG_MN), and Shape index (SHAPE_MN). At the class level, 19 2-D landscape metrics were generated. Cluster analysis and backward selection algorithms were applied to eliminate redundancy. As a result, the following metrics that showed strong correlations (>0.70) were excluded: Largest patch index (LPI), Total edge (TE), Mean Shape index (SHAPE_MN), Perimeter-area ratio (PARA_MN), Landscape shape index (LSI), Patch cohesion index (COHESION), Division index (DIVISION), Effective mesh size (MESH), and Aggregation index (AI). As a result, 30 class-level landscape metrics (10 metrics multiplied by three land use classes) were used, including building, asphalt, and tree land covers. For the 3-D landscape metrics, 16 were derived from 3-D information from buildings and vegetation data, and twelve were used (Table A2): Building Height (3D-Hb), Vegetation height (3D-Hv), Sky view factor (3D-SVF), Building volume (3D-Bv), Aboveground biomass (3D-AGB), Building height coefficient of variation (3D-CVb), Vegetation height coefficient of variation (3D-CVv), Compactness for building height (3D-Cb), Building height evenness index (3D-BEI), Vegetation height evenness index (3D-VEI), Building height patch index (3D-PRb), Vegetation height patch index (3D-PRv).

The main factors affecting MRT were determined by evaluating the 2-D and 3-D landscape metrics separately and combined through stepwise multiple regression analysis. The results are presented in Table 1, which shows the standardized regression coefficients that demonstrate a significant relationship between dependent and independent variables. A positive relationship between MRT and 2-D and 3-D landscape metrics at 8.00 h, 12:00 h, and 16:00 h becomes negative at 20:00 h and vice versa. MRT responds positively to 2D-l-CONTAG and 2D-l-SHAPE_MN during the day and negatively at 20:00 h. On the other hand, 2D-l-FRAC_MN, 2D-l-ED, and 2D-l-SPLIT exhibit negative responses at 8:00 h, 12:00 h, and 16:00 h and positive responses at 20:00 h. 2D-l-MESH shows a positive response at 8:00 h and 12:00 h but no correlation at 16:00 h and 20:00 h. On the other hand, 2D-l-CONTIG_MN shows a negative response at 8:00 h and 12:00 h but no significant correlation at 16:00 h and 20:00 h. Conversely, 2D-l-NP has a positive correlation at 16:00 h and 20:00 h and no correlation at other hours. In contrast, 2D-l-PD provides a positive correlation only at 16:00 h.

The stepwise regression analysis for the selected 2-D metrics at the landscape level revealed R-squared (R^2) values between 0.32 and 0.35 for hourly MRT. Each model's R^2 and adjusted R^2 values were less than 0.70, indicating that the model is unreliable for interpreting the results. The relative importance of each metric in the model is 2D-SPLIT > 2D-l-SHAPE_MN > 2D-FRAC_MN ~ 2D-CONTAG > 2D-l-ED > 2D-l-CONTIG_MN > 2D-l-MESH > 2D-l-NP > 2D-l-PD. These metrics, generally referring to landscape configuration, were weakly correlated with MRT at the landscape level.

At the class level, 2D-C-ED_Building, 2D-C-C-CONTIG_MN_Building, 2D-C-CONTIG_MN_Trees, and 2D-C-PAFRAC_MN_Building display a positive correlation with MRT during daytime and a negative correlation after sunset. Conversely, 2D-C-PLAND_Building, 2D-C-PLAND_Trees, and 2D-C-ED_Asphalt are negatively correlated during the day and positively correlated at night. The remaining class-level metrics do not exhibit a significant correlation with MRT. In particular, 2D-C-PAFRAC_MN_Trees and 2D-C-FRAC_MN_Asphalt show positive correlations between 08:00 h and 12:00 h, whereas 2D-C-PD_Asphalt shows negative and positive correlations between 16:00 h and 20:00 h. There is also a significant low-impact correlation between the metrics 2D-C-CA_Asphalt, 2D-C-CA_Building, 2D-C-PLAND_Asphalt, 2D-C-NP_Trees, and 2D-C-PD_Trees, usually at 8:00 h or 20:00 h.

For the 3D building and vegetation metrics, MRT is positively correlated with 3D-CVb, 3D-CVv, 3D-Bv, 3D-SVF, and 3D-AGB during daytime hours and negatively correlated with the other 3-D metrics. This relationship reverses at 20:00 h. MRT is collinear with the 3D-SVF variable at all hours with a VIF greater than 7.5. Therefore, the SVF was excluded from the stepwise multiple regression analysis. The model accuracy between MRT and 3-D metrics varies between 71 % to 87 %, indicating a high correlation. The lowest R^2 accuracy occurred at 8:00 h, while the highest occurred at noon. Vegetation-related metrics were more significant than building height metrics. The relative importance levels are as follows: 3D-Hv>3D-CVv>3D-BEI>3D-Bv>3D-AGB>3D-CVb>3D-PRb>3D-PRv>3D-Hb. The strongest correlation for the 3D-Hv and 3D-BEI metrics occurs at 12:00 h when solar radiation is closest to its peak, and the average MRT is the highest. However, there is no significant correlation with the 3D-Hb metric because building shadows are minimal at these hours.

Multiple regression with 2D and 3D landscape metrics yields model accuracies between 86 % and 96 %. This strong relationship indicates the necessity of using both horizontal and vertical data in an integrated manner. The variable importance is as follows: 3D-Hv > 2D-C-PLAND_Tree > 3D-Hb > 3D-CVv > 2D-C-ED_Building > 2D-l-PD > 3D-VEI > 2D-C-ED_Asphalt > 2D-C-CLUMPY_Tree > 2D-C-PAFRAC_MN_Tree > 2D-C-CLUMPY_Building > 3D-Bv > 3D-BEI. The R^2 for a regression using the five metrics with the strongest relationship in the model (3D-Hv > 2D-C-PLAND_Tree > 3D-Hb > 3D-CVv > 2D-C-ED_Building) at 08:00 h, 12:00 h, 16:00 h, and 20:00 h is 0.82, 0.95, 0.88 and 0.91, respectively. This result shows that 3D-Hv (vegetation height), 2D-C-PLAND_Tree (percentage of tree cover), 3D-Hb (building height), and 2D-C-ED_Building (Building edge density) have a significant negative correlation with MRT during the daytime as they characterize how much direct solar radiation an urban surface receives. In contrast, they have a positive correlation after sunset.

4. Discussion

The stepwise regression analysis results indicate a negative correlation between MRT, 2D-C-ED, and 2D-SPLIT metrics during the daytime hours. This outcome aligns with findings from previous research studies (Kwon & Lee, 2019; Zhang et al., 2022). ED measures the diversity of the landscape, while SPLIT measures the density of discrete regions. High values of ED and SPLIT positively influence MRT at the urban scale. In our study, ED exhibits a strong negative correlation with LPI, while it has a high positive correlation with DIVISION and all aggregation indices. These metrics take a similar approach to ED, and research conducted by Zhang et al. (2022), Chen et al. (2020), Li et al. (2020), and Wang et al. (2020) support this grouping.

Our results confirm that the thermal environment in urban areas is influenced by various factors, including building height, vegetation, and other urban landscape elements (Oke, 1989). Our regression analysis of the 3-D landscape metrics revealed that vegetation height had the most substantial negative relationship. No significant association was found for building height at 12:00 h and 16:00 h. Since most of the study area consists of 2-story residential buildings with wide roads, these areas have less shade from buildings, and plant height affects MRT more than buildings.

The five most important 3-D factors explaining MRT at all times of the day are 3D-Hv, 2D-C-PLAND_Tree, 3D-Hb, 2D-C-ED_Building, and 3D-CVv metrics. Except for 3D-CVv, these metrics have a significant negative correlation with MRT, consistent with previous studies (Chen et al., 2014; Li et al., 2012). Similar to the 2D metrics, 3D metrics related to vegetation and building height have a significant negative daytime and positive nighttime effect on MRT. They characterize how much direct solar radiation an urban surface can receive (Alavipanah et al., 2018). Increasing building or vegetation height throughout the day increases shading, thus reducing the heat storage of surfaces in the urban canyon. However, vegetation traps more longwave radiation from the ground at night. On the other hand, the 3D-CVv (vegetation height coefficient of variation) metric has a significant positive correlation with MRT during the daytime, while the relationship is reversed at night.

Building edge density at 2-D and 3-D scales reduces MRT by

increasing landscape diversity, producing more shade patterns. However, this relationship increases the building surface area and leads to the absorption of more solar radiation that is dissipated to the environment at night, increasing nighttime warming (Huang & Wang, 2019; Jamei & Rajagopalan, 2017). Dense urban areas also have poor ventilation, causing more heat retention at night (Alexander, 2021; Lin et al., 2017; Sun et al., 2020a). We also found that high MRT values are clustered predominantly in large open areas. Conversely, clusters of low MRT values are concentrated in city centers with tall buildings and more vegetated neighborhoods.

Increasing the number of trees and water bodies and reducing impervious surfaces effectively cools the urban environment, but the implementation can be challenging in hot, arid areas such as Phoenix and Tempe. Instead of changing the landscape composition, urban planners can consider optimizing the configuration of urban landscapes as an alternative cooling approach (Zheng et al., 2014). According to Li et al. (2011), the spatial configuration of different land cover types significantly affects the UTE. In our study, vegetation height, percentage of tree cover, and coefficient of variation of vegetation height were the critical factors for MRT concerning vegetation cover, supporting these previous findings. Building and edge density in cities had the largest impact on MRT because more complex building shapes create more

Table 1
The stepwise regression analysis results between multi-dimensional landscape metrics and MRT after eliminating collinear variables at four hours of interest (8:00h, 12:00h, 16:00h, and 20:00h).

Times	8:00h			12:00h			16:00h			20:00h		
	UC (Std. Error)	SC*	VIF	UC (Std. Error)	SC*	VIF	UC (Std. Error)	SC*	VIF	UC (Std. Error)	SC*	VIF
2-D Variables (Landscape level)												
(Constant)	53.132 (0.899)			69.225 (0.624)			75.79 (1.070)			27.992 (0.444)		
2D-L-SHAPE_MN	1.663 (0.134)	0.42	2.66	1.061 (0.093)	0.27	2.66	1.941 (0.171)	0.50	1.94	-0.856 (0.07)	-0.22	1.83
2D-L-FRAC_MN	-8.691 (0.765)	-0.36	2.33	-5.871 (0.531)	-0.25	2.33	-10.442 (0.979)	-0.44	1.71	4.733 (0.402)	0.20	1.62
2D-L-CONTIG_MN	-0.886 (0.200)	-0.12	1.71	-0.858 (0.139)	-0.12	1.71			4			
2D-L-ED	-0.001 (0.000)	-0.31	4.08	-0.001 (0.000)	-0.13	4.08	0.000 (0.000)	-0.29	1.24	0.000 (0.000)	0.13	3.92
2D-L-NP							0.000 (0.000)	0.17		0.000 (0.000)	-0.08	1.24
2D-L-PD							0.000 (0.000)	0.14	1.23			
2D-L-CONTAG	0.023 (0.003)	0.24	3.47	0.019 (0.002)	0.20	3.47	0.0555 (0.005)	0.58	3.38	-0.022 (0.002)	-0.24	3.37
2D-L-MESH	0.071 (0.011)	0.13	1.1	0.0357 (0.008)	0.07	1.1						
2D-L-SPLIT	-0.063 (0.003)	-0.48	1.46	-0.049 (0.002)	-0.37	1.46	-0.112 (0.005)	-0.85	1.61	0.051 (0.002)	0.39	1.61
R^2	0.34			0.32			0.33			0.35		
Adjusted R^2	0.34			0.32			0.33			0.35		
2-D Variables (Class level)												
(Constant)	46.262 (0.586)			63.359 (0.155)			68.907 (0.238)			31.337 (0.106)		
2D-C-CA-Asphalt	0.032 (0.006)	0.07	1.24									
2D-C-CA-Building										-0.091 (0.012)	-0.09	3.89
2D-C-PLAND_Building	-0.060 (0.001)	-0.57	1.69	-0.023 (0.001)	-0.23	1.57	-0.084 (0.002)	-0.08	1.57	0.043 (0.001)	0.04	2.09
2D-C-PLAND_Trees	-0.169 (0.002)	-1.25	1.6	-0.144 (0.001)	-1.06	1.36	-0.281 (0.002)	-0.28	1.32	0.127 (0.001)	0.00	1.44
2D-C-PLAND_Asphalt										0.003 (0.000)	0.13	2.68
2D-C-ED-Building	0.000 (0.000)	0.14	2.32	0.000 (0.000)	0.11	1.73	0.001 (0.000)	0.00	1.78	0.000 (0.000)	0.00	2.24
2D-C-ED-Asphalt	-0.001 (0.000)	-0.24	1.19	0.000 (0.000)	-0.16	1.15	-0.001 (0.000)	0.00	1.25	0.000 (0.000)	0.00	2.08
2D-C-NP-Trees										0.000 (0.000)	0.00	3.57
2D-C-PD-Trees	0.000 (0.000)	-0.13	1.99									
2D-C-PD-Asphalt							0.000 (0.000)	0.00	1.27	0.000 (0.000)	0.00	1.30
2D-C-FRAC_MN-Building	-1.384 (0.379)	-0.06	1.45									
2D-C-FRAC_MN-Asphalt	0.606 (0.153)	0.06	1.16	0.321 (0.083)	0.03	1.09						
2D-C-CONTIG_MN-Building	2.153 (0.247)	0.15	1.68	1.547 (0.123)	0.11	1.30	3.411 (0.290)	3.41	1.36	-1.693 (0.127)	-1.69	1.36
2D-C-CONTIG_MN-Trees	0.906 (0.176)	0.08	1.47	0.853 (0.092)	0.08	1.28	1.500 (0.214)	1.50	1.27	-0.735 (0.094)	-0.74	1.30

(continued on next page)

Table 1 (*continued*)

2D-C-PAFRAC_MN-Building	0.032 (0.008)	0.05	1.08	0.019 (0.004)	0.03	1.07	0.048 (0.01)	0.05	1.06	-0.018 (0.004)	-0.02	1.07
2D-C-PAFRAC_MN-Trees	0.274 (0.050)	0.08	1.27	0.157 (0.026)	0.05	1.16						
R^2	0.70			0.81			0.77			0.78		
Adjusted R^2	0.70			0.81			0.77			0.78		
3-D Variables												
(Constant)	46.36 (0.064)			64.577 (0.031)			70.335 (0.086)			30.666 (0.039)		
3D-Hb	-0.055 (0.016)	-0.09	4.22							0.035 (0.008)	0.06	4.22
3D-Hv	-3.012 (0.045)	-1.12	1.66	-2.611 (0.021)	-0.97	1.65	-4.959 (0.059)	-1.84	1.65	2.226 (0.024)	0.83	1.66
3D-Bv	0.001 (0.000)	0.16	1.6	0.001 (0)	0.08	1.29	0.001 (0.000)	0.15	1.27	-0.001 (0.000)	-0.10	1.6
3D-AGB	0.343 (0.0356)	0.15	1.46	0.094 (0.016)	0.04	1.47	0.291 (0.047)	0.13	1.46	-0.161 (0.019)	-0.07	1.53
3D-CVb	0.008 (0.001)	0.12	1.37	0.005 (0.001)	0.08	1.32				-0.002 (0.000)	-0.04	1.4
3D-CVv	0.093 (0.006)	0.23	1.33	0.057 (0.002)	0.15	1.31	0.136 (0.007)	0.34	1.3	-0.055 (0.003)	-0.14	1.33
3D-BEI	-1.048 (0.065)	-0.33	2.51	-0.198 (0.026)	-0.06	1.9	-1.583 (0.069)	-0.50	1.63	0.610 (0.034)	0.19	2.52
3D-PRb	-0.012 (0.002)	-0.13	2.67	-0.01 (0.001)	-0.10	2.66	-0.023 (0.002)	-0.23	2.64	0.010 (0.001)	0.10	3.63
3D-PRv				0.009 (0.001)	0.06	2.14	0.017 (0.003)	0.11	2.08	-0.005 (0.001)	-0.04	2.14
R^2	0.72			0.87			0.78			0.81		
Adjusted R2	0.71			0.87			0.78			0.81		
2-D and 3-D Variables												
(Constant)	41.476 (0.610)			63.298 (0.132)			69.177 (0.709)			32.105 (0.209)		
2D-C-CA-Building	0.069 (0.009)	0.08	1.58									
2D-C-ED-Asphalt	0.000 (0.000)	-0.10	1.4	0.000 (0.000)	-0.05	1.3	0.000 (0.000)	-0.14	1.34	-0.035 (0.004)	-0.04	1.53
2D-C-ED-Building	0.000 (0.000)	-0.21	2.34	0.000 (0.000)	-0.09	2.57	0.000 (0.000)	-0.24	2.79	0.000 (0.000)	0.07	1.35
2D-C-CLUMPY-Building	1.355 (0.266)	0.06	1.55	0.628 (0.106)	0.03	2.04	1.701 (0.490)	0.07	3.62	0.000 (0.000)	0.06	2.37
2D-C-CLUMPY-Trees	2.794 (0.300)	0.11	1.76	0.858 (0.111)	0.03	2.01	2.275 (0.386)	0.09	2.01	-1.103 (0.117)	-0.05	1.55
2D-C-SPLIT-Building							0.000 (0.000)	-0.07	2.47	-1.342 (0.141)	-0.05	2.02
2D-C-FRAC_MN-Building							-1.029 (0.321)	-0.04	1.25	0.538 (0.115)	0.02	1.2
2D-C-FRAC_MN-Asphalt	0.394 (0.107)	0.04	1.2									
2D-C-FRAC_MN-Trees	1.773 (0.360)	0.05	1.22									
2D-C-CONTIG_MN-Building				0.231 (0.068)	0.01	1.7						
2D-C-CONTIG_MN-Trees				-0.319 (0.056)	-0.03	2.57	-1.04 (0.194)	-0.09	2.54	0.454 (0.070)	0.04	2.54
2D-C-PLAND_Trees	-0.035 (0.003)	-0.26	7.37	-0.029 (0.001)	-0.21	7.13	-0.078 (0.003)	-0.58	6.82	0.027 (0.001)	0.21	7.43
2D-C-PAFRAC_MN-Trees	0.333 (0.038)	0.10	1.49	0.121 (0.012)	0.04	1.4	0.275 (0.044)	0.08	1.36	-0.189 (0.016)	-0.06	1.39
2D-L-SHAPE_MN	-0.979 (0.119)	-0.12	2.51									
2D-L-PD	0.000 (0.000)	-0.18	3.1	0.000 (0.000)	-0.05	2.54	0.000 (0.000)	-0.12	2.5	0.000 (0.000)	0.08	2.5
2D-L-SPLIT										0.002 (0.000)	0.02	1.92

(*continued on next page*)

Table 1 (*continued*)

3D-Hb	-0.172 (0.012)	-0.29	5.29	-0.085 (0.004)	-0.14	4.67	-0.274 (0.011)	-0.46	3.17	0.113 (0.005)	0.19	5.29
3D-Hv	-1.731 (0.066)	-0.58	5.84	-1.925 (0.023)	-0.65	6.14	-3.539 (0.08)	-1.19	5.96	1.374 (0.029)	0.46	6.07
3D-Bv	0.000 (0.000)	0.05	1.77	0.000 (0.000)	0.03	1.69	0.000 (0.000)	0.07	1.71	0.000 (0.000)	-0.04	1.78
3D-CVb				0.002 (0.000)	0.02	1.47						
3D-CVv	0.263 (0.011)	0.37	3.12	0.124 (0.004)	0.18	3.15	0.207 (0.013)	0.29	3.13	-0.157 (0.005)	-0.22	3.16
3D-Cb							-0.001 (0.000)	-0.04	1.07			
3D-BEI	-0.322 (0.062)	-0.09	3.69	0.317 (0.020)	0.09	3.2	-0.395 (0.071)	-0.11	3.39	0.237 (0.027)	0.07	3.68
3D_VEI	-0.570 (0.077)	-0.13	3.7	-0.379 (0.026)	-0.09	3.69	-0.489 (0.090)	-0.11	3.51	0.379 (0.032)	0.09	3.52
3D-PRb	-0.001 (0.001)	-0.10	3.7	-0.004 (0.000)	-0.05	3.69				0.006 (0.000)	0.06	2.73
3D-PRv	-0.007 (0.002)	-0.05	2.47	0.002 (0.000)	0.02	2.37						
R^2	0.86			0.96			0.91			0.94		
Adjusted R^2	0.86			0.96			0.90			0.94		

Note: UC stands for unstandardized coefficient; SC stands for standardized coefficient * Sig. level $p<0.001$

shade than compact, simple structures. According to our results, 2-D and 3-D characteristics of buildings and vegetation significantly affect the UTE. Therefore, studying the relative differences in buildings and vegetation under different urban form scenarios is essential for urban planners to create optimal UTEs in cities.

Urban green spaces regulate the UTE through shading and evapotranspiration (Liu et al., 2017b; Tan et al., 2021; Unal Cilek & Cilek, 2021; Wang et al., 2021). Kong et al. (2022) found that above-ground biomass (AGB) negatively correlates with daytime MRT in Nanjing, China. The importance of AGB in mitigating the UHI effects has been emphasized in numerous studies (Deng et al., 2018; Wang et al., 2021). However, the low biomass presence in Arizona was not significantly correlated with MRT in the model using all metrics. While several studies have reported the cooling effects of urban green spaces on the thermal environment, the interactions between AGB and other factors in regulating the thermal environment remain unclear. More studies are needed to investigate the role of AGB in heterogeneous locations.

Comprehensive knowledge of landscape metric impacts on MRT is necessary for developing effective UTE improvement strategies. Our multiple regression incorporating 2-D and 3-D metrics shows high explanatory power ranging from 86 % to 96 %, suggesting that using a combination of horizontal and vertical data is crucial. Using the most relative five metrics with the strongest relationship in the model (3D-Hv > 2D-C-PLAND_Tree > 3D-Hb > 3D-CVv > 2D-C-ED_Building) can achieve an accuracy ranging from 82 % to 95 %, indicating that considering only these metrics is sufficient.

4.1. Limitations

Our analysis of the hierarchical variation and interaction effects in the relationship between various landscape metrics and MRT has several limitations. First, the study was confined to summer. Identifying the spatial hierarchy of all landscape metrics is crucial based on their seasonal characteristics, and future research should consider other seasons.

Second, while MRT is used to assess the spatial distribution of an experienced heat load on the body, calculating Physiological Equivalent Temperature (PET) or other more comprehensive indices would be needed to evaluate the impact of landscape metrics on human thermal comfort. However, calculating PET at high resolution in the area is challenging because the index combines multiple meteorological variables (wind speed, relative humidity, air temperature) that are unknown at high resolution and would have to be modeled. MRT works well as a proxy for human thermal exposure in hot and dry places such as Phoenix, while PET will be more representative in areas with high humidity (Hu et al., 2020; Middel & Krayenhoff, 2019).

Lastly, the high-resolution MRT data used in our study was calculated without land cover considerations. Future research should include high-resolution classified land cover to examine the impact of different surface materials on MRT.

4.2. Implication for urban planning and design

Our results offer important insights into the dynamics of thermal exposure and land system architecture (Turner et al. 2013) that can inform passive cooling strategies in urban planning and design. First, our 2-D and 3-D landscape metrics show that the impact of urban morphology on pedestrian-experienced intra-urban heat is dynamic and changes between day and night. Some metrics correlate positively with MRT during the day and negatively at night, and vice versa, illustrating tradeoffs that are inherent in urban design; strategies that reduce thermal exposure during the day, such as urban densification, will increase thermal loads after sunset due to longwave trapping. In an urban design process, it is important to decide what times of day should be prioritized for cooling depending on space use. Second, vegetation, especially tree height (3D-Hv), is important for shading pedestrians in residential neighborhoods with wide roads and large setbacks, such as LCZ 6 in Phoenix and Tempe. These neighborhoods should be targeted for tree planting if resources are available.

We found that the most significant drivers of MRT are building and vegetation height, percent tree coverage, and edge density of buildings. While it seems obvious that taller buildings and trees (vertical urban features) increase shade production, our study is the first to show that increased landscape diversity decreases thermal exposure during the day. Complex buildings produce more shade than square or rectangular structures of the same area coverage, offering great potential for passive cooling.

5. Conclusions

Tree planting can be challenging in hot, arid areas such as Phoenix and Tempe. Instead of changing the landscape composition and increasing the vegetated fraction, our study shows that diversifying the 3-D configuration of the built environment yields additional passive cooling. Using stepwise multiple regression, we investigated the

hierarchical exchange and interaction effects of 2-D and 3-D landscape metrics with MRT. We found a weak correlation between MRT and 2-D landscape metrics at the landscape level, but when 2-D and 3-D metrics were combined, a highly significant correlation with MRT was found at various times of the day. The impact of average building and vegetation height on MRT depends on the location, environment, and time. Building and vegetation height has a significant influence on MRT, exhibiting a noteworthy negative response. During the day, shade from tall vertical urban features reduced surface temperatures and heat storage in the urban fabric, but the building edge density (i.e., the complexity of the building shape) also positively contributed to urban cooling at the hyperlocal scale. Similarly, tall vegetation contributes to MRT reduction by blocking shortwave radiation. Our results provide a new perspective on managing urban form for thermally comfortable and livable environments using 3-D configuration and composition metrics. The study emphasizes the need to consider the complex relationships between urban landscapes and MRT in designing and planning sustainable urban environments and suggests that more complex, heterogeneous built environments are cooler than homogeneous landscapes due to increased shading. Insights from this study can guide urban planners and designers to develop passive cooling strategies, create more thermally comfortable outdoor environments, and reduce energy consumption in buildings.

CRediT authorship contribution statement

Ahmet Cilek: Conceptualization, Data curation, Formal analysis, Investigation, Methodology, Software, Supervision, Validation, Visualization, Writing – original draft. **Muge Unal:** Conceptualization, Data curation, Methodology, Software, Validation, Visualization, Writing – original draft, Writing – review & editing. **Ariane Middel:** Conceptualization, Data curation, Funding acquisition, Methodology, Project administration, Supervision, Writing – review & editing.

Declaration of Competing Interest

The authors declare that they have no known competing financial interests or personal relationships that could have appeared to influence the work reported in this paper.

Data availability

Data will be made available on request.

Acknowledgments

This work was supported by the National Science Foundation, grant number CMMI-1942805 (CAREER: Human Thermal Exposure in Cities - Novel Sensing and Modeling to Build Heat-Resilience). Any opinions, findings, conclusions, or recommendations expressed in this material are those of the authors and do not necessarily reflect the views of the sponsoring organizations.

Supplementary materials

Supplementary material associated with this article can be found, in the online version, at doi:10.1016/j.scs.2023.105116.

References

Alavipanah, S., Schreyer, J., Haase, D., Lakes, T., & Qureshi, S. (2018). The effect of multi-dimensional indicators on urban thermal conditions. *Journal of Cleaner Production, 177*, 115–123. https://doi.org/10.1016/J.JCLEPRO.2017.12.187

Alberti, M., & Marzluff, J. M. (2004). Ecological resilience in urban ecosystems: Linking urban patterns to human and ecological functions. *Urban Ecosystems, 7*(3), 241–265. https://doi.org/10.1023/B:UECO.0000044038.90173.C6

Alexander, C. (2021). Influence of the proportion, height and proximity of vegetation and buildings on urban land surface temperature. *International Journal of Applied Earth Observation and Geoinformation, 95*, Article 102265. https://doi.org/10.1016/J.JAG.2020.102265

Amiri, R., Weng, Q., Alimohammadi, A., & Alavipanah, S. K. (2009). Spatial–temporal dynamics of land surface temperature in relation to fractional vegetation cover and land use/cover in the Tabriz urban area, Iran. *Remote Sensing of Environment, 113*, 2606–2617. https://doi.org/10.1016/J.RSE.2009.07.021

Asgarian, A., Amiri, B. J., & Sakieh, Y. (2015). Assessing the effect of green cover spatial patterns on urban land surface temperature using landscape metrics approach. *Urban Ecosystems, 18*, 209–222. https://doi.org/10.1007/S11252-014-0387-7/TABLES/4

Baker, W. L., & Cai, Y. (1992). The r.le programs for multiscale analysis of landscape structure using the GRASS geographical information system. *Landscape Ecology, 7*, 291–302. https://doi.org/10.1007/BF00131258/METRICS

Berger, C., Rosentreter, J., Voltersen, M., Baumgart, C., Schmullius, C., & Hese, S. (2017). Spatio-temporal analysis of the relationship between 2D/3D urban site characteristics and land surface temperature. *Remote Sensing of Environment, 193*, 225–243. https://doi.org/10.1016/J.RSE.2017.02.020

Bhaduri, B., Minner, M., Tatalovich, S., & Harbor, J. (2001). Long-term hydrologic impact of urbanization: A tale of two models. *Journal of Water Resources Planning and Management, 127*, 13–19. https://doi.org/10.1061/(ASCE)0733-9496(2001)127:1(13)

Bivand, R., & Piras, G. (2015). Comparing implementations of estimation methods for spatial econometrics. *Journal of Statistical Software, 63*, 1–36. https://doi.org/10.18637/JSS.V063.I18

Bowler, D. E., Buyung-Ali, L., Knight, T. M., & Pullin, A. S. (2010). Urban greening to cool towns and cities: A systematic review of the empirical evidence. *Landscape and Urban Planning, 97*, 147–155. https://doi.org/10.1016/J.LANDURBPLAN.2010.05.006

Brazel, A., Selover, N., Vose, R., & Heisler, G. (2000). The tale of two climates-Baltimore and Phoenix urban LTER sites. *Research; A Journal of Science and its Applications, 15*, 123–135. https://doi.org/10.2307/24867306

Buo, I., Sagris, V., Jaagus, J., & Middel, A. (2023). High-resolution thermal exposure and shade maps for cool corridor planning. *Sustainable Cities and Society, 93*, Article 104499. https://doi.org/10.1016/J.SCS.2023.104499

Cai, D., Fraedrich, K., Guan, Y., Guo, S., & Zhang, C. (2017). Urbanization and the thermal environment of Chinese and US-American cities. *Science of The Total Environment, 589*, 200–211. https://doi.org/10.1016/J.SCITOTENV.2017.02.148

Charalampopoulos, I., Tsiros, I., Chronopoulou-Sereli, A., & Matzarakis, A. (2013). Analysis of thermal bioclimate in various urban configurations in Athens, Greece. *Urban Ecosystems, 16*, 217–233. https://doi.org/10.1007/S11252-012-0252-5/FIGURES/11

Chen, A., Yao, L., Sun, R., & Chen, L. (2014). How many metrics are required to identify the effects of the landscape pattern on land surface temperature? *Ecological Indicators, 45*, 424–433. https://doi.org/10.1016/J.ECOLIND.2014.05.002

Chen, A., Zhao, X., Yao, L., & Chen, L. (2016). Application of a new integrated landscape index to predict potential urban heat islands. *Ecological indicators, 69*, 828–835.

Chen, S., Jiang, H., Chen, Y., & Cai, Z. (2020). Spatial-temporal patterns of net primary production in Anji (China) between 1984 and 2014. *Ecological Indicators, 110*, Article 105954. https://doi.org/10.1016/j.ecolind.2019.105954

Chen, X., Zhao, P., Hu, Y., Ouyang, L., Zhu, L., & Ni, G. (2019). Canopy transpiration and its cooling effect of three urban tree species in a subtropical city- Guangzhou, China. *Urban Forestry and Urban Greening, 43*, Article 126368. https://doi.org/10.1016/J.UFUG.2019.126368

Chow, W. T. L., Chuang, W. C., & Gober, P. (2012). Vulnerability to extreme heat in metropolitan Phoenix: Spatial, temporal, and demographic dimensions. *The Professional Geographer, 64*, 286–302. https://doi.org/10.1080/00330124.2011.600225

Chow, W. T. L., Chuang, W.-C., & Gober, P. (2011). The professional geographer vulnerability to extreme heat in metropolitan Phoenix: spatial, temporal, and demographic dimensions. *The Professional Geographer, 64*, 286–302. https://doi.org/10.1080/00330124.2011.600225

Chun, B., & Guldmann, J. M. (2018). Impact of greening on the urban heat island: Seasonal variations and mitigation strategies. *Computers, Environment and Urban Systems, 71*, 165–176. https://doi.org/10.1016/J.COMPENVURBSYS.2018.05.006

Deilami, K., Kamruzzaman, M., & Liu, Y. (2018). Urban heat island effect: A systematic review of spatio-temporal factors, data, methods, and mitigation measures. *International Journal of Applied Earth Observation and Geoinformation, 67*, 30–42. https://doi.org/10.1016/J.JAG.2017.12.009

Deng, L., Mao, Z., Li, X., Hu, Z., Duan, F., & Yan, Y. (2018). UAV-based multispectral remote sensing for precision agriculture: A comparison between different cameras. *ISPRS Journal of Photogrammetry and Remote Sensing, 146*, 124–136. https://doi.org/10.1016/j.isprsjprs.2018.09.008

Duh, J. Der, Shandas, V., Chang, H., & George, L. A. (2008). Rates of urbanisation and the resiliency of air and water quality. *Science of The Total Environment, 400*, 238–256. https://doi.org/10.1016/J.SCITOTENV.2008.05.002

Estoque, R. C., Murayama, Y., & Myint, S. W. (2017). Effects of landscape composition and pattern on land surface temperature: An urban heat island study in the megacities of Southeast Asia. *Science of The Total Environment, 577*, 349–359. https://doi.org/10.1016/J.SCITOTENV.2016.10.195

Frazier, A. E., & Kedron, P. (2017). Landscape metrics: Past progress and future directions. *Current Landscape Ecology Reports 2017, 2*(3 2), 63–72. https://doi.org/10.1007/S40823-017-0026-0

Fu, W. J., Jiang, P. K., Zhou, G. M., & Zhao, K. L. (2014). Using Moran's i and GIS to study the spatial pattern of forest litter carbon density in a subtropical region of

southeastern China. *Biogeosciences (Online), 11*, 2401–2409. https://doi.org/10.5194/BG-11-2401-2014

Gal, C. V., & Kantor, N. (2020). Modeling mean radiant temperature in outdoor spaces, A comparative numerical simulation and validation study. *Urban Climate, 32* (December 2019), Article 100571. https://doi.org/10.1016/j.uclim.2019.100571

Getzner, M., Färber, B., & Yamu, C. (2016). 2D Versus 3D: The Relevance of the Mode of Presentation for the Economic Valuation of an Alpine Landscape. *Sustainability, 8*, 591. https://doi.org/10.3390/SU8060591

Guo, A., Yang, J., Xiao, X., Xia (Cecilia), J., Jin, C., & Li, X. (2020). Influences of urban spatial form on urban heat island effects at the community level in China. *Sustainable Cities and Society, 53*, Article 101972. https://doi.org/10.1016/J.SCS.2019.101972

Guo, G., Wu, Z., & Chen, Y. (2019). Complex mechanisms linking land surface temperature to greenspace spatial patterns: Evidence from four southeastern Chinese cities. *Science of The Total Environment, 674*, 77–87. https://doi.org/10.1016/J.SCITOTENV.2019.03.402

Han, L., Zhou, W., Li, W., & Li, L. (2014). Impact of urbanization level on urban air quality: A case of fine particles (PM2.5) in Chinese cities. *Environmental Pollution, 194*, 163–170. https://doi.org/10.1016/J.ENVPOL.2014.07.022

Harlan, S. L., Brazel, A. J., Prashad, L., Stefanov, W. L., & Larsen, L. (2006). Neighborhood microclimates and vulnerability to heat stress. *Social Science & Medicine (1982), 63*, 2847–2863. https://doi.org/10.1016/J.SOCSCIMED.2006.07.030

Hondula, D. M., Georgescu, M., & Balling, R. C. (2014). Challenges associated with projecting urbanization-induced heat-related mortality. *Science of The Total Environment, 490*, 538–544. https://doi.org/10.1016/J.SCITOTENV.2014.04.130

Hu, Y., Dai, Z., & Guldmann, J. M. (2020). Modeling the impact of 2D/3D urban indicators on the urban heat island over different seasons: A boosted regression tree approach. *Journal of Environmental Management, 266*. https://doi.org/10.1016/J.JENVMAN.2020.110424

Huang, X., & Wang, Y. (2019). Investigating the effects of 3D urban morphology on the surface urban heat island effect in urban functional zones by using high-resolution remote sensing data: A case study of Wuhan, Central China. *ISPRS Journal of Photogrammetry and Remote Sensing, 152*, 119–131. https://doi.org/10.1016/J.ISPRSJPRS.2019.04.010

Jamei, E., & Rajagopalan, P. (2017). Urban development and pedestrian thermal comfort in Melbourne. *Solar Energy, 144*, 681–698. https://doi.org/10.1016/J.SOLENER.2017.01.023

Johansson, E., & Emmanuel, R. (2006). The influence of urban design on outdoor thermal comfort in the hot, humid city of Colombo, Sri Lanka. *International Journal of Biometeorology, 51*, 119–133. https://doi.org/10.1007/S00484-006-0047-6/FIGURES/13

Kalnay, E., & Cai, M. (2003). Impact of urbanization and land-use change on climate. *Nature, 423*(6939), 528–531. https://doi.org/10.1038/nature01675

Kalnay, E., Cai, M., Karl, T. R., Williams, C. N., Young, P. J., Wendland, W. M., & Easterling, D. R. (2004). Impact of land-use change on climate. *Nature, 427*(6971), 214. https://doi.org/10.1038/427214a

Kane, K., Connors, J. P., & Galletti, C. S. (2014). Beyond fragmentation at the fringe: A path-dependent, high-resolution analysis of urban land cover in Phoenix, Arizona. *Applied Geography, 52*, 123–134. https://doi.org/10.1016/J.APGEOG.2014.05.002

Ke, B., Hu, W., Huang, D., Zhang, J., Lin, X., Li, C., Jin, X., & Chen, J. (2022). Three-dimensional building morphology impacts on PM2.5 distribution in urban landscape settings in Zhejiang, China. *Science of The Total Environment, 826*, Article 154094. https://doi.org/10.1016/J.SCITOTENV.2022.154094

Kelly Turner, V., Middel, A., & Vanos, J. K. (2023). Shade is an essential solution for hotter cities. *Nature, 619*, 694–697. https://doi.org/10.1038/d41586-023-02311-3

Kong, F., Chen, J., Middel, A., Yin, H., Li, M., Sun, T., Zhang, N., Huang, J., Liu, H., Zhou, K., & Ma, J. (2022). Impact of 3-D urban landscape patterns on the outdoor thermal environment: A modelling study with SOLWEIG. *Computers, Environment and Urban Systems, 94*. https://doi.org/10.1016/j.compenvurbsys.2022.101773

Kottek, M., Grieser, J., Beck, C., Rudolf, B., & Rubel, F. (2006). World map of the Köppen–Geiger climate classification updated. *Meteorologische Zeitschrift, 15*, 259–263. https://doi.org/10.1127/0941-2948/2006/0130

Kwon, Y. J., & Lee, D. K. (2019). Thermal comfort and longwave radiation over time in urban residential complexes. *Sustainability, 11*, 2251. https://doi.org/10.3390/su11082251

Li, J., Song, C., Cao, L., Zhu, F., Meng, X., & Wu, J. (2011). Impacts of landscape structure on surface urban heat islands: A case study of Shanghai, China. *Remote Sensing of Environment, 115*, 3249–3263. https://doi.org/10.1016/J.RSE.2011.07.008

Li, T., Xu, Y., & Yao, L. (2021). Detecting urban landscape factors controlling seasonal land surface temperature: from the perspective of urban function zones. *Environmental Science and Pollution Research, 28*, 41191–41206. https://doi.org/10.1007/s11356-021-13695-y

Li, X., Li, W., Middel, A., Harlan, S. L., Brazel, A. J., & Turner, B. L. (2016). Remote sensing of the surface urban heat island and land architecture in Phoenix, Arizona: Combined effects of land composition and configuration and cadastral–demographic–economic factors. *Remote Sensing of Environment, 174*, 233–243. https://doi.org/10.1016/J.RSE.2015.12.022

Li, X., Zhou, W., Ouyang, Z., Xu, W., & Zheng, H. (2012). Spatial pattern of greenspace affects land surface temperature: Evidence from the heavily urbanized Beijing metropolitan area, China. *Landscape Ecology, 27*, 887–898. https://doi.org/10.1007/S10980-012-9731-6/FIGURES/4

Li, Y., Schubert, S., Kropp, J. P., & Rybski, D. (2020). On the influence of density and morphology on the Urban Heat Island intensity. *Nature Communications, 11*(1), 1–9. https://doi.org/10.1038/s41467-020-16461-9

Lin, P., Lau, S. S. Y., Qin, H., & Gou, Z. (2017). Effects of urban planning indicators on urban heat island: A case study of pocket parks in high-rise high-density environment. *Landscape and Urban Planning, 168*, 48–60. https://doi.org/10.1016/J.LANDURBPLAN.2017.09.024

Lindberg, F., Holmer, B., & Thorsson, S. (2008). SOLWEIG 1.0 – Modelling spatial variations of 3D radiant fluxes and mean radiant temperature in complex urban settings. *International Journal of Biometeorology, 52*, 697–713. https://doi.org/10.1007/s00484-008-0162-7

Liu, M., Hu, Y. M., & Li, C. L. (2017a). Landscape metrics for three-dimensional urban building pattern recognition. *Applied Geography, 87*, 66–72. https://doi.org/10.1016/J.APGEOG.2017.07.011

Liu, W., Feddema, J., Hu, L., Zung, A., & Brunsell, N. (2017b). Seasonal and diurnal characteristics of land surface temperature and major explanatory factors in Harris County, Texas. *Sustainability 2017, 9*, 2324. https://doi.org/10.3390/SU9122324

Luan, Q., Jiang, W., Liu, S., & Guo, H. (2020). Impact of Urban 3D morphology on particulate matter 2.5 (PM2.5) concentrations: case study of Beijing, China. *Chinese Geographical Science / Sponsored by Changchun Institute of Geography, Chinese Academy of Sciences, 30*, 294–308. https://doi.org/10.1007/S11769-020-1112-5/METRICS

Masoudi, M., Tan, P. Y., & Fadaei, M. (2021). The effects of land use on spatial pattern of urban green spaces and their cooling ability. *Urban Climate, 35*, Article 100743. https://doi.org/10.1016/J.UCLIM.2020.100743

McGarigal, K., Cushman, S., Neel, M., & Ene, E. (2002). *FRAGSTATS: Spatial pattern analysis program for categorical maps*. URL http://www.umass.edu/landeco/research/fragstats/fragstats.html (accessed 4.3.23).

Middel, A., AlKhaled, S., Schneider, F. A., Hagen, B., & Coseo, P. (2021). 50 grades of shade. *Bulletin of the American Meteorological Society, 102*, E1805–E1820. https://doi.org/10.1175/BAMS-D-20-0193.1

Middel, A., Häb, K., Brazel, A. J., Martin, C. A., & Guhathakurta, S. (2014). Impact of urban form and design on mid-afternoon microclimate in Phoenix Local Climate Zones. *Landscape and Urban Planning, 122*, 16–28. https://doi.org/10.1016/J.LANDURBPLAN.2013.11.004

Middel, A., & Krayenhoff, E. S. (2019). Micrometeorological determinants of pedestrian thermal exposure during record-breaking heat in Tempe, Arizona: Introducing the MaRTy observational platform. *Science of The Total Environment, 687*, 137–151. https://doi.org/10.1016/J.SCITOTENV.2019.06.085

Middel, A., Lukasczyk, J., Maciejewski, R., Demuzere, M., & Roth, M. (2018). Sky view factor footprints for urban climate modeling. *Urban Climate, 25*, 120–134. https://doi.org/10.1016/J.UCLIM.2018.05.004

Middel, A., Selover, N., Hagen, B., & Chhetri, N. (2016). Impact of shade on outdoor thermal comfort—A seasonal field study in Tempe, Arizona. *International Journal of Biometeorology, 60*, 1849–1861. https://doi.org/10.1007/S00484-016-1172-5/FIGURES/9

Myint, S. W., Wentz, E. A., Brazel, A. J., & Quattrochi, D. A. (2013). The impact of distinct anthropogenic and vegetation features on urban warming. *Landscape Ecology, 28*, 959–978. https://doi.org/10.1007/S10980-013-9868-Y/TABLES/5

National Weather Service. (2018). *NWS phoenix, n.d.National weather service - NWS Phoenix*. Phoenix.

Nichol, J. E. (1996). High-resolution surface temperature patterns related to urban morphology in a tropical city: A satellite-based study. *Journal of Applied Meteorology and Climatology, 35*(1), 135–146.

Norton, B. A., Coutts, A. M., Livesley, S. J., Harris, R. J., Hunter, A. M., & Williams, N. S. G. (2015). Planning for cooler cities: A framework to prioritise green infrastructure to mitigate high temperatures in urban landscapes. *Landscape and Urban Planning, 134*, 127–138. https://doi.org/10.1016/J.LANDURBPLAN.2014.10.018

Oke, T. R. (1989). The micrometeorology of the urban forest. *Philosophical Transactions - Royal Society of London, B, 324*, 335–349. https://doi.org/10.1098/rstb.1989.0051

Oke, T. R., Mills, G., Christen, A., & Voogt, J. A. (2017). *Urban climates* (pp. 1–525). https://doi.org/10.1017/9781139016476

Papagiannaki, K., Lagouvardos, K., Kotroni, V., & Bezes, A. (2015). Flash flood occurrence and relation to the rainfall hazard in a highly urbanized area. *Natural Hazards and Earth System Sciences, 15*, 1859–1871. https://doi.org/10.5194/NHESS-15-1859-2015

Perkins, S. E., Alexander, L. V., & Nairn, J. R. (2012). Increasing frequency, intensity and duration of observed global heatwaves and warm spells. *Geophysical Research Letters, 39*, 20714. https://doi.org/10.1029/2012GL053361

Petras, V., Newcomb, D. J., & Mitasova, H. (2017). Generalized 3D fragmentation index derived from lidar point clouds. *Open Geospatial Data, Software and Standards, 2*(1), 1–14. https://doi.org/10.1186/S40965-017-0021-8

Ratti, C., Di Sabatino, S., & Britter, R. (2006). Urban texture analysis with image processing techniques: Winds and dispersion. *Theoretical and Applied Climatology, 84*, 77–90. https://doi.org/10.1007/S00704-005-0146-Z/METRICS

Santamouris, M. (2013). Using cool pavements as a mitigation strategy to fight urban heat island—A review of the actual developments. *Renewable and Sustainable Energy Reviews, 26*, 224–240. https://doi.org/10.1016/J.RSER.2013.05.047

Schneider, F. A., Ortiz, J. C., Vanos, J. K., Sailor, D. J., & Middel, A. (2023). Evidence-based guidance on reflective pavement for urban heat mitigation in Arizona. *Nature Communications 2023, 14*(1), 1–12. https://doi.org/10.1038/s41467-023-36972-5

Szucs, A., Gal, T., & Andrade, H. (2014). Comparison of measured and simulated mean radiant temperature. Case study in Lisbon (Portugal). *Finisterra, 49*(98), 95–111. https://doi.org/10.18055/Finis6469

Sha, M., & Tian, G. (2010). An analysis of spatiotemporal changes of urban landscape pattern in Phoenix metropolitan region. *Procedia Environmental Sciences, 2*, 600–604. https://doi.org/10.1016/J.PROENV.2010.10.066

Shen, C., Hou, H., Zheng, Y., Murayama, Y., Wang, R., & Hu, T. (2022). Prediction of the future urban heat island intensity and distribution based on landscape composition

and configuration: A case study in Hangzhou. *Sustainable Cities and Society, 83*. https://doi.org/10.1016/j.scs.2022.103992
Shrestha, M. K., York, A. M., Boone, C. G., & Zhang, S. (2012). Land fragmentation due to rapid urbanization in the Phoenix Metropolitan Area: Analyzing the spatiotemporal patterns and drivers. *Applied Geography, 32*, 522–531. https://doi.org/10.1016/J.APGEOG.2011.04.004
Siqi, J., & Yuhong, W. (2020). Effects of land use and land cover pattern on urban temperature variations: A case study in Hong Kong. *Urban Climate, 34*, Article 100693. https://doi.org/10.1016/J.UCLIM.2020.100693
Solcerova, A., van de Ven, F., Wang, M., Rijsdijk, M., & van de Giesen, N. (2017). Do green roofs cool the air? *Built Environment, 111*, 249–255. https://doi.org/10.1016/J.BUILDENV.2016.10.021
Stevens, J. P. (2009). *Applied multivariate statistics for the social sciences* (4th Ed). New York: Routledge.
Stewart, I. D., & Oke, T. R. (2012). Local Climate Zones for Urban Temperature Studies. *Bulletin of the American Meteorological Society, 93*, 1879–1900.
Sun, F., Liu, M., Wang, Y., Wang, H., & Che, Y. (2020a). The effects of 3D architectural patterns on the urban surface temperature at a neighborhood scale: Relative contributions and marginal effects. *Journal of Cleaner Production, 258*, Article 120706. https://doi.org/10.1016/J.JCLEPRO.2020.120706
Sun, Y., Gao, C., Li, J., Li, W., & Ma, R. (2018). Examining urban thermal environment dynamics and relations to biophysical composition and configuration and socio-economic factors: A case study of the Shanghai metropolitan region. *Sustainable Cities and Society, 40*, 284–295. https://doi.org/10.1016/J.SCS.2017.12.004
Sun, Y., Wang, S., & Wang, Y. (2020b). Estimating local-scale urban heat island intensity using nighttime light satellite imageries. *Sustainable Cities and Society, 57*, Article 102125. https://doi.org/10.1016/J.SCS.2020.102125
Tan, X., Sun, X., Huang, C., Yuan, Y., & Hou, D. (2021). Comparison of cooling effect between green space and water body. *Sustainable Cities and Society, 67*, Article 102711. https://doi.org/10.1016/J.SCS.2021.102711
Tian, Y., Zhou, W., Qian, Y., Zheng, Z., & Yan, J. (2019). The effect of urban 2D and 3D morphology on air temperature in residential neighborhoods. *Landscape Ecology, 34*, 1161–1178.
Thorsson, S., Lindberg, F., Eliasson, I., & Holmer, B. (2007). Different methods for estimating the mean radiant temperature in an outdoor urban setting. *International Journal of Climatology, 27*, 1983–1993. https://doi.org/10.1002/JOC.1537
Turner, B. L., et al. (2013). *Land system architecture: Using land systems to adapt and mitigate global environmental change. no. PNNL-SA-93482*. Pacific Northwest National Lab.(PNNL)Richland, WA (United States).
Unal Cilek, M., & Cilek, A. (2021). Analyses of land surface temperature (LST) variability among local climate zones (LCZs) comparing Landsat-8 and ENVI-met model data. *Sustainable Cities and Society, 69*, Article 102877. https://doi.org/10.1016/j.scs.2021.102877
Unger, J. (2009). Connection between urban heat island and sky view factor approximated by a software tool on a 3D urban database. *International Journal of Environment and Pollution, 36*, 59–80. https://doi.org/10.1504/IJEP.2009.021817
Wang, C., Middel, A., Myint, S. W., Kaplan, S., Brazel, A. J., & Lukasczyk, J. (2018). Assessing local climate zones in arid cities: The case of Phoenix, Arizona and Las Vegas, Nevada. *ISPRS Journal of Photogrammetry and Remote Sensing, 141*, 59–71. https://doi.org/10.1016/J.ISPRSJPRS.2018.04.009
Wang, J. L., Zhang, Y. H., Shao, M., Liu, X. L., Zeng, L. M., Cheng, C. L., & Xu, X. F. (2006). Quantitative relationship between visibility and mass concentration of PM2.5 in Beijing. *Journal of Environmental Sciences, 18*, 475–481.
Wang, L., Hou, H., & Weng, J. (2020). Ordinary least squares modelling of urban heat island intensity based on landscape composition and configuration: A comparative study among three megacities along the Yangtze River. *Sustainable Cities and Society, 62*, Article 102381. https://doi.org/10.1016/J.SCS.2020.102381
Wang, Z., Meng, Q., Allam, M., Hu, D., Zhang, L., & Menenti, M. (2021). Environmental and anthropogenic drivers of surface urban heat island intensity: A case-study in the Yangtze River Delta, China. *Ecological Indicators, 128*, Article 107845. https://doi.org/10.1016/J.ECOLIND.2021.107845
Wang, Z., Ishida, Y., & Mochida, A. (2023). Effective factors for reducing land surface temperature in each local climate zone built type in Tokyo and Shanghai. *Remote Sens, 15*(15), 3840.
Western Regional Climate Center, 2020. Historical Climate Information. URL https://wrcc.dri.edu/cgi-bin/cliMAIN.pl?az8499 [WWW Document].
Wong, N. H., & Yu, C. (2005). Study of green areas and urban heat island in a tropical city. *Habitat International, 29*, 547–558. https://doi.org/10.1016/J.HABITATINT.2004.04.008
Wu, Q., Guo, F., Li, H., & Kang, J. (2017). Measuring landscape pattern in three dimensional space. *Landscape and Urban Planning, 167*, 49–59. https://doi.org/10.1016/J.LANDURBPLAN.2017.05.022
Wu, Z., Wei, L., & Lv, Z. (2012). Landscape Pattern Metrics: An Empirical Study from 2-D to 3-D. *Physical Geography, 33*, 383–402. https://doi.org/10.2747/0272-3646.33.4.383
Xian, G., & Crane, M. (2006). An analysis of urban thermal characteristics and associated land cover in Tampa Bay and Las Vegas using Landsat satellite data. *Remote Sensing of Environment, 104*, 147–156. https://doi.org/10.1016/J.RSE.2005.09.023
Xiao, R., Cao, W., Liu, Y., & Lu, B. (2022). The impacts of landscape patterns spatio-temporal changes on land surface temperature from a multi-scale perspective: A case study of the Yangtze River Delta. *Science of the Total Environment, 821*. https://doi.org/10.1016/j.scitotenv.2022.153381
Yan, J., Zhou, W., & Jenerette, G. D. (2019). Testing an energy exchange and microclimate cooling hypothesis for the effect of vegetation configuration on urban heat. *Agricultural and Forest Meteorology, 279*, Article 107666. https://doi.org/10.1016/J.AGRFORMET.2019.107666
Yin, J., Wu, X., Shen, M., Zhang, X., Zhu, C., Xiang, H., Shi, C., Guo, Z., & Li, C. (2019). Impact of urban greenspace spatial pattern on land surface temperature: A case study in Beijing metropolitan area, China. *Landscape Ecology, 34*, 2949–2961. https://doi.org/10.1007/S10980-019-00932-6/TABLES/6
Yu, Q., Acheampong, M., Pu, R., Landry, S. M., Ji, W., & Dahigamuwa, T. (2018). Assessing effects of urban vegetation height on land surface temperature in the City of Tampa, Florida, USA. *International Journal of Applied Earth Observation and Geoinformation, 73*, 712–720. https://doi.org/10.1016/J.JAG.2018.08.016
Yu, S., Chen, Z., Yu, B., Wang, L., Wu, B., Wu, J., & Zhao, F. (2020). Exploring the relationship between 2D/3D landscape pattern and land surface temperature based on explainable eXtreme Gradient Boosting tree: A case study of Shanghai, China. *Science of the Total Environment, 725*. https://doi.org/10.1016/j.scitotenv.2020.138229
Yu, S., Yu, B., Song, W., Wu, B., Zhou, J., Huang, Y., Wu, J., Zhao, F., & Mao, W. (2016). View-based greenery: A three-dimensional assessment of city buildings' green visibility using Floor Green View Index. *Landscape and Urban Planning, 152*, 13–26. https://doi.org/10.1016/J.LANDURBPLAN.2016.04.004
Yu, X., Liu, Y., Zhang, Z., & Xiao, R. (2021). Influences of buildings on urban heat island based on 3D landscape metrics: An investigation of China's 30 megacities at micro grid-cell scale and macro city scale. *Landscape Ecology, 36*, 2743–2762. https://doi.org/10.1007/s10980-021-01275-x
Zellweger, F., De Frenne, P., Lenoir, J., Rocchini, D., & Coomes, D. (2019). Advances in microclimate ecology arising from remote sensing. *Trends Ecology and Evolution, 34*, 327–341. https://doi.org/10.1016/J.TREE.2018.12.012
Zeng, P., Sun, F., Liu, Y., Tian, T., Wu, J., Dong, Q., Peng, S., & Che, Y. (2022). The influence of the landscape pattern on the urban land surface temperature varies with the ratio of land components: Insights from 2D/3D building/vegetation metrics. *Sustainable Cities and Society, 78*. https://doi.org/10.1016/j.scs.2021.103599
Zhan, X., Liang, X., Xu, G., & Zhou, L. (2013). Influence of plant root morphology and tissue composition on phenanthrene uptake: Stepwise multiple linear regression analysis. *Environmental Pollution, 179*, 294–300. https://doi.org/10.1016/J.ENVPOL.2013.04.033
Zhang, D., Zhou, C., Zhou, Y., & Zikirya, B. (2022). Spatiotemporal relationship characteristic of climate comfort of urban human settlement environment and population density in China. *Frontiers in Ecology and Evolution, 10*, Article 953725. https://doi.org/10.3389/fevo.2022.953725
Zhang, Y., Middel, A., & Turner, B. L. (2019). Evaluating the effect of 3D urban form on neighborhood land surface temperature using Google Street View and geographically weighted regression. *Landscape Ecology, 34*, 681–697. https://doi.org/10.1007/S10980-019-00794-Y/FIGURES/5
Zhang, Y. Z., Sun, C., Bao, Y., & Zhou, Q. (2018). How surface roughness reduces heat transport for small roughness heights in turbulent Rayleigh–Bénard convection. *Journal of Fluid Mechanics, 836*, R2. https://doi.org/10.1017/JFM.2017.786
Zheng, B., Myint, S. W., & Fan, C. (2014). Spatial configuration of anthropogenic land cover impacts on urban warming. *Landscape and Urban Planning, 130*, 104–111. https://doi.org/10.1016/J.LANDURBPLAN.2014.07.001
Zhou, L., Hu, F., Wang, B., Wei, C., Sun, D., & Wang, S. (2022a). Relationship between urban landscape structure and land surface temperature: Spatial hierarchy and interaction effects. *Sustainable Cities and Society, 80*. https://doi.org/10.1016/j.scs.2022.103795
Zhou, W., Wang, J., & Cadenasso, M. L. (2017). Effects of the spatial configuration of trees on urban heat mitigation: A comparative study. *Remote Sensing of Environment, 195*, 1–12. https://doi.org/10.1016/J.RSE.2017.03.043
Zhou, Y., Zhao, H., Mao, S., Zhang, G., Jin, Y., Luo, Y., Huo, W., Pan, Z., An, P., & Lun, F. (2022b). Exploring surface urban heat island (SUHI) intensity and its implications based on urban 3D neighborhood metrics: An investigation of 57 Chinese cities. *Science of the Total Environment, 847*. https://doi.org/10.1016/j.scitotenv.2022.157662
Zimble, D. A., Evans, D. L., Carlson, G. C., Parker, R. C., Grado, S. C., & Gerard, P. D. (2003). Characterizing vertical forest structure using small-footprint airborne LiDAR. *Remote Sensing of Environment, 87*, 171–182. https://doi.org/10.1016/S0034-4257(03)00139-1
Zhang, Y., & Turner, B. II. (2020). Land-cover mapping of the central Arizona region based on 2015 National Agriculture Imagery Program (NAIP) imagery ver 1. *Environmental Data Initiative*. https://doi.org/10.6073/pasta/e671ed549a55fda3338b177a2ad54487